

Regional and Temporal Variability of Lateral Mixing in the North Atlantic

THOMAS BOLTON

Atmospheric, Oceanic, and Planetary Physics, University of Oxford, Oxford, United Kingdom

RYAN ABERNATHEY

Lamont-Doherty Earth Observatory, Columbia University, Palisades, New York

LAURE ZANNA

Department of Physics, University of Oxford, Oxford, United Kingdom

(Manuscript received 18 February 2019, in final form 9 July 2019)

ABSTRACT

Geostrophic eddies contribute to the mixing of heat, carbon, and other climatically important tracers. A passive tracer driven by satellite-derived surface velocity fields is used to study the regional and temporal variability of lateral eddy mixing in the North Atlantic. Using a quasi-Lagrangian diffusivity diagnostic, we show that the upstream region (80°–50°W) of the Gulf Stream jet exhibits a significant mixing barrier (with diffusivity of $\approx 1 \times 10^3 \text{ m}^2 \text{ s}^{-1}$), compared to the downstream region (50°–10°W), which displays no mixing suppression ($\approx 10 \times 10^3 \text{ m}^2 \text{ s}^{-1}$). The interannual variability is 10%–20% of the time mean in both regions. By analyzing linear perturbations of mixing-length diffusivity expression, we show that the across-jet mixing in the upstream region is driven by variations in the mean flow, rather than eddy velocity. In the downstream region, both the mean flow and eddy velocity contribute to the temporal variability. Our results suggest that an eddy parameterization must take into account the along-jet variation of mixing, and within jets such diffusivities may be a simple function of jet strength.


1. Introduction

Mesoscale eddies, of length scales of 10–100 km, are ubiquitous in the global ocean and dominate the oceanic kinetic energy (Ferrari and Wunsch 2009; Wortham and Wunsch 2014). These turbulent mesoscale eddies derive their energy from barotropic and baroclinic instabilities, and through scale interactions play a key role in setting the global ocean circulation (e.g., Schmittner and Weaver 2001; Chapman and Sallée 2017). Mesoscale eddies impact the stirring, mixing, and transport of important climatic tracers such as heat, salinity, and carbon (e.g., Gnanadesikan et al. 2015). Atmospheric forcing can also contribute significantly to intergyre exchange (Yang and Liu 1994; Yang 1996); here, however, we

focus solely on the impact of internal ocean dynamics on surface mixing.

Mesoscale eddies modify lateral tracer mixing through stirring (i.e., advection which conserves tracer concentration) and the subsequent modification of tracer gradients. The tracer mixing is typically quantified by an eddy diffusivity, which measures the amount of tracer flux per unit tracer gradient. However, a more energetic mesoscale eddy field does not necessarily lead to increased eddy diffusivities, due to the phenomena of “mixing barriers.” While there is no strict definition of mixing barriers, these are typically characterized by a significant suppression of the eddy diffusivity (e.g., Nakamura 1996; Klocker et al. 2012).

Mixing barriers can also be identified by higher-order statistical moments of dynamical quantities. For examples, Hughes et al. (2010) showed that mixing barriers

 Denotes content that is immediately available upon publication as open access.

Corresponding author: Thomas Bolton, tom.bolton@physics.ox.ac.uk



This article is licensed under a Creative Commons Attribution 4.0 license (<http://creativecommons.org/licenses/by/4.0/>).

DOI: 10.1175/JPO-D-19-0042.1

© 2019 American Meteorological Society

Unauthenticated | Downloaded 08/09/22 08:15 AM UTC

lead to specific patterns spatial patterns of skewness (third centralized moment, measuring the asymmetry of a distribution) and kurtosis (fourth centralized moment, measuring how “fat-tailed” a distribution is) in observations of vorticity and sea level. Mixing barriers lead to a sign change in skewness, moving across the mixing barrier. While kurtosis exhibits a local minimum, due to fluctuations about the mean position of the mixing barrier. Therefore, higher-order statistical moments can provide information on whether tracers (active or passive) are being mixed.

Mixing barriers are typically caused by the presence of zonal jets, where the strong mean flow produces a sharp coherent front, reducing or suppressing mixing despite the presence of turbulent eddies. An illustrative example is the Antarctic Circumpolar Current (ACC) in the Southern Ocean. The zonal jets of the ACC cause the across-jet diffusivity to drop significantly (Shuckburgh et al. 2009; Ferrari and Nikurashin 2010, hereafter FN10; Klocker et al. 2012) despite the energetic mesoscale eddy field.

Within the North Atlantic, the presence of strong mean flows and mesoscale eddies lead to competing effects, similar to the ACC: eddies generally act to increase lateral mixing through enhanced tracer gradients, whereas strong mean flows lead to mixing barriers that suppress diffusivities. Bower et al. (1985) showed that within the Gulf Stream region, cross-frontal mixing is indeed suppressed at the surface. At the surface, the amplitude of the jet meandering impacts the amount of cross-frontal exchange (Bower and Rossby 1989; Bower 1991; Samelson 1992), where jet meandering affects the mixing barrier suppression of the mean flow. Reduced intergyre exchange across the Gulf Stream is observed for sea surface temperature (SST) anomalies (Foukal and Lozier 2016).

The goal of this study is to quantify and understand in more detail the spatial variability of surface lateral mixing in the North Atlantic. Mesoscale eddies are present across all of the North Atlantic, but their dynamical impact varies with along-stream position (as shown by Waterman et al. 2011; Waterman and Hoskins 2013). We therefore expect the impact on the lateral mixing of tracers to also vary regionally, especially within western boundary currents such as the Gulf Stream.

Across-jet transport within the Gulf Stream has already been shown to depend on longitude (Liu et al. 2018, their Fig. 12), where the Gulf Stream transitions from an unstable jet to the wave-maker regime (Waterman and Jayne 2010). Here we investigate how larger regional variations—length scales greater than $\mathcal{O}(1000)$ km—in mesoscale eddy dynamics impacts the lateral mixing of tracers. In particular, we compare diffusivities in the

vicinity of the Gulf Stream (west of 50°W), to diffusivities diagnosed downstream in the presence of the more diffusive North Atlantic and Azores Currents (east of 50°W).

To investigate the regional variation of eddy diffusivities, we employ a global observation-driven passive tracer experiment (Marshall et al. 2006; Abernathey and Marshall 2013; Klocker and Abernathey 2014; Busecke et al. 2017; Busecke and Abernathey 2019). Surface ocean velocities from satellite altimetry data are used to evolve a passive tracer, from which we diagnose effective diffusivities using the framework of Nakamura (1996). These effective diffusivities are used as an indicator of true lateral mixing in the North Atlantic. We then test the theoretical diffusivity expression of FN10 against the effective diffusivities estimates, and then see what dynamical properties of the flow contribute to the interannual variability.

We find contrasting behavior in the effective diffusivity between the upstream and downstream regions (defined in section 2c) of the North Atlantic. Upstream exhibits significant mixing suppression ($\approx 1000 \text{ m}^2 \text{ s}^{-1}$) in the jet core of the Gulf Stream, while downstream, in the presence of the North Atlantic and Azores Currents, exhibits a single large peak ($\approx 10000 \text{ m}^2 \text{ s}^{-1}$) in the effective diffusivity. The interannual variability of both regions is approximately 10%–20% of the time mean (over a 21-yr period). In the upstream region the FN10 expressions reproduces the mixing suppression observed in the effective diffusivity, and we find that the interannual variability is dominated by changes in the magnitude of the mean flow. In the downstream region, we find that the FN10 expression does not capture the large peak of the effective diffusivity and underestimates mixing in this region.

This paper is structured as follows: section 2 describes the satellite altimetry data, the passive tracer simulations, and the definitions of the upstream and downstream regions; in section 3 we investigate the regional and temporal variability of the effective diffusivity, including the analysis of the mixing length diffusivity expression of FN10; in section 4 we link the upstream effective diffusivity to the dynamics of the Gulf Stream jet; and in section 5 we discuss the implications of our results and avenues for further work.

2. Data and methods

a. AVISO satellite altimetry data

We use two “level 4” gridded products from AVISO altimetry data (<https://www.aviso.altimetry.fr/en/data.html>): absolute dynamic topography (ADT) and surface geostrophic

velocities derived from ADT. ADT is formed by combining the mean dynamic topography (MDT) with sea level anomalies (SLA); MDT is the ocean topography due to the mean currents, relative to the geoid, and SLA are the satellite measurements of the oceans anomalous surface height. The surface velocities are derived from sea surface height data by assuming geostrophy. After an optimal interpolation procedure (Le Traon et al. 1998), the products have $1/4^\circ \times 1/4^\circ$ spatial resolution on a Mercator grid, with daily data beginning from 1993.

b. Passive tracer model

To conduct a numerical passive tracer experiment driven by observations, we use MITgcm (Marshall et al. 1997; Adcroft et al. 2008) in “offline” mode. The AVISO geostrophic velocities only measure velocities at the surface, so it is a single layer experiment run globally. Before running the model, the AVISO geostrophic surface velocities $\mathbf{u} = (u, v)$ are adjusted to be nondivergent, which corresponds to a 1% correction. A nondivergent velocity field is necessary in order to conserve the passive tracer. Weekly time slices of the surface velocities are linearly interpolated to each time step of the model, and spatially integrated to a $1/10^\circ$ grid. The following two-dimensional advection–diffusion equation is then solved for the passive tracer field q

$$\frac{\partial q}{\partial t} + (\mathbf{u} \cdot \nabla)q = \kappa \nabla^2 q, \quad (1)$$

where t is time, κ is a prescribed horizontal diffusivity, and $\nabla = (\partial/\partial x, \partial/\partial y)$ is the horizontal gradient. The passive tracer experiment depends upon the initial tracer distribution $q(t = 0)$, and the value of the horizontal diffusivity κ ; the sensitivity to both these factors are discussed in Abernathey and Marshall (2013), where various initializations are tested, as well as values of κ ranging from 25 to $150 \text{ m}^2 \text{ s}^{-1}$.

Based on the results of Abernathey and Marshall (2013), we initialize the passive tracer on the time-mean streamfunction (averaged over the ≈ 20 -yr period of available data) such that the initial field is as aligned as possible with the mean flow. Any subsequent induced tracer variance by the flow will therefore be due to transient flows. Initializing on the time-mean streamfunction also reduces the initial “shock” of the passive tracer to the underlying velocities, and within the Gulf Stream the adjustment takes less than 4 weeks.

After many eddy lifetimes, the global tracer variance will decrease as the time-mean tracer flux will be directed downgradient. The tracer is therefore reinitialized every year to avoid complete homogenization. Reinitializing the passive tracer at the beginning of each

year also improves the study of the interannual variability, as the initial adjustment then occurs within each year.

c. Upstream and downstream regions

To determine how the dynamics within the North Atlantic impact lateral mixing, and how the lateral mixing varies along stream, we define two regions: upstream as 80° – 50°W , and downstream as 50° – 10°W , with both between 30° and 60°N in latitude. The two regions are shown in Figs. 1a and 1b, with the gray dotted line illustrating the boundary between the upstream and downstream regions.

The upstream is characterized by the presence of the Gulf Stream jet, a coherent current that separates from the coast at Cape Hatteras at 35°N , after which the jet meanders eastward. The strong mean flow in the upstream region produces a sharp front, also known as the Gulf Stream North Wall, argued to act as a barrier to mixing at the surface (Bower et al. 1985).

In the downstream region, the Gulf Stream jet evolves into the North Atlantic Current and the Azores Current (Rossby 1996), the former transporting warm tropical waters to high latitudes, and the latter flowing in a southeasterly direction contributing to transport within the subtropical gyre. The North Atlantic Current and the Azores Current do not produce as sharp a front as the Gulf Stream jet, but both the upstream and downstream regions exhibit an energetic mesoscale eddy field that contributes to the lateral mixing of tracers.

3. North Atlantic lateral tracer mixing

a. Tracer statistical moments

To illuminate the time-mean behavior of the passive tracer in the North Atlantic, we calculate the first four statistical moments of the passive tracer and compare them to observations of an active tracer, namely SST (Fig. 1). We use SST observations from the ARMOR3D dataset (Guinehut et al. 2012) and remove the seasonal cycle at each grid point. Each statistical moment helps describe properties of the tracer probability distribution function (PDF), and the first four moments are the following: mean, standard deviation, skewness, and kurtosis. The standard deviation measures the width of the PDF and is therefore a measure of the temporal variability, skewness is a measure of the asymmetry of the PDF, and kurtosis indicates how probability is distributed between the peak and tails of the PDF and relates to the frequency of extreme values.

The mean of both the SST and passive tracer exhibit a sharp front—characterized by large meridional gradients—in the upstream region, where there is a strong coherent jet. The mean fields of SST and the passive tracer in the downstream region are more diffuse, as the Gulf Stream

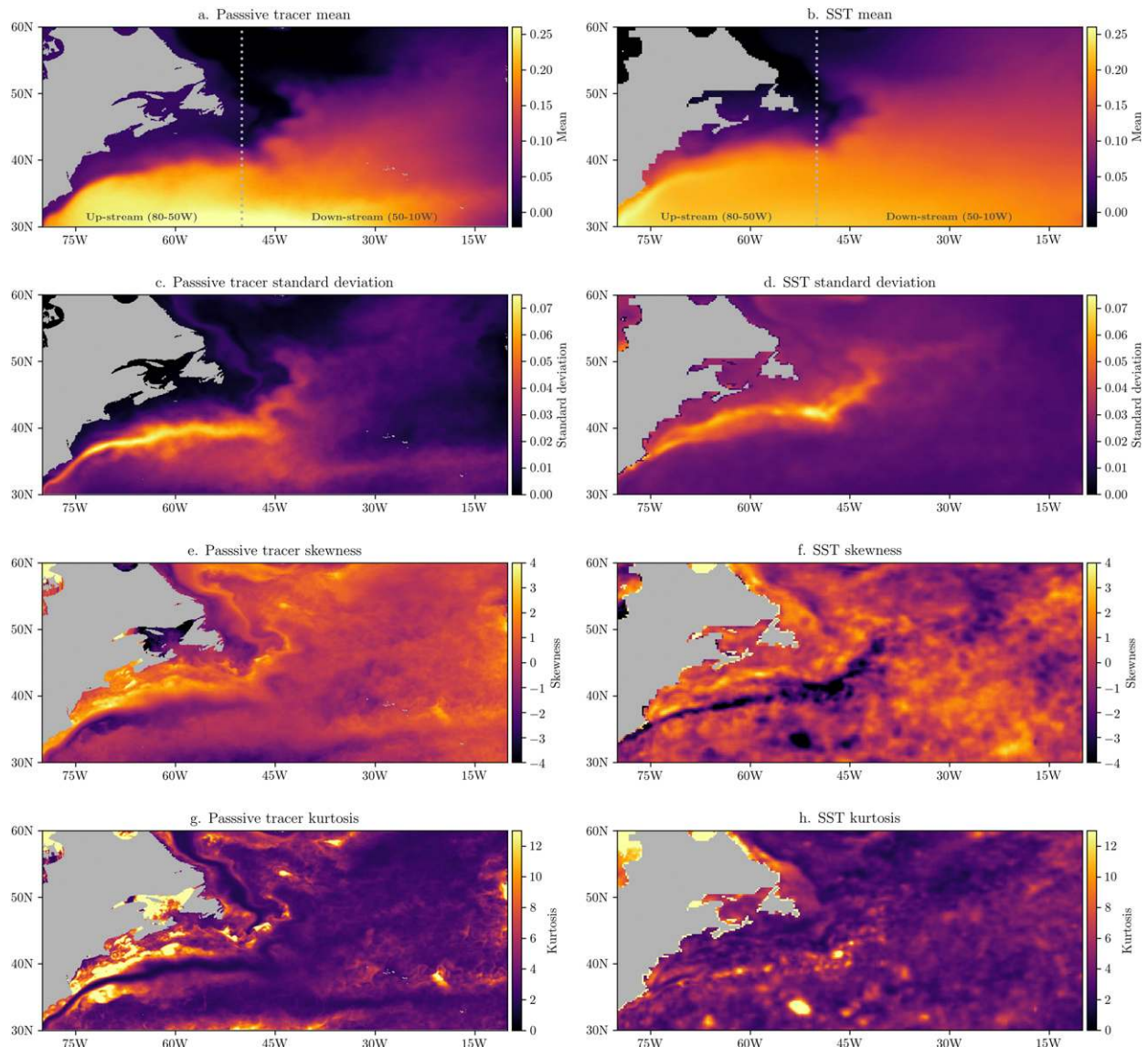


FIG. 1. The first four statistical moments of SST and the passive tracer q by sampling values at each point in space. The rows from top to bottom represent the four statistical moments: (a),(b) mean, (c),(d) standard deviation, (e),(f) skewness, and (g),(h) kurtosis; (left) 22 years of passive tracer data, and (right) SST observations over the same period. SST data is from the ARMOR3D dataset (Guinehut et al. 2012). The mean and standard deviation have units of tracer concentration (or $^{\circ}\text{C}$ for SST), while the skewness and kurtosis are dimensionless. The upstream and downstream regions (80° – 50° and 50° – 10°W , respectively), are illustrated in (a) and (b).

jet evolves into the less-vigorous North Atlantic Current and Azores Current. The standard deviation is dominated by the Gulf Stream jet in the upstream region, with an order of magnitude more variance than in the downstream region. The skewness of both the SST and passive tracer undergo a sign change moving across the jet in the upstream region. The skewness sign change is indicative of a mixing barrier, as discussed in Hughes et al. (2010) and David et al. (2017); the latitude of zero skewness represents the mean-jet position, as it is the latitude at which the jet core is equally likely to be above

or below that point. The passive tracer kurtosis displays a high–low–high pattern moving across the jet, also indicative of a mixing barrier. However, the SST kurtosis does not show this high–low–high pattern, potentially due to interactions unique to an active tracer like SST, which is not captured by the passive tracer field.

The statistical moments indicate that, at least in the time-mean evolution of SST and the passive tracer, there are important dynamical differences between the upstream and downstream regions. In addition, except for the kurtosis, the passive tracer exhibits qualitatively

similar statistics to the SST field. Any insight gained by studying passive tracer mixing can then hopefully generalize to climatic tracers in the North Atlantic.

b. Effective diffusivity and tracer flux

Eddy mixing involves the enhancement of tracer gradients due to the conservative stirring of the eddy advection. The conservative stirring deforms tracer contours into finer spatial structures, from which the background horizontal diffusivity κ becomes significant and homogenizes the tracer. The mixing produced through this mechanism can be represented with an eddy diffusivity K_{eddy} . One measure of eddy mixing by enhanced tracer gradients is the Osborn–Cox diffusivity (Osborn and Cox 1972), which measures the enhancement of tracer gradients relative to the background gradients $K_{\text{OC}} = |\nabla q|^2 / |\nabla \bar{q}|^2$, where \bar{x} denotes the time mean and x' denotes the deviation from the time mean.

However, the Osborn–Cox diffusivity K_{OC} calculates the tracer gradients in an Eulerian manner at each point in space. When applied to a system such as the Gulf Stream, large anomalous tracer gradients $|\nabla q|^2$ produced simply from the latitudinal shifts in the meandering jet can strongly affect the estimates of diffusivity, despite not contributing to irreversible mixing.

We therefore use the effective diffusivity K_{eff} of Nakamura (1996), a quasi-Lagrangian diagnostic of mixing that also considers the magnitude of tracer gradients, but using the tracer area A as a coordinate system. The tracer area $A = A(q)$ is the total area of the tracer below the contour q [a visual explanation of the area coordinate can be found in Fig. 1 of Nakamura (1996)]. The effective diffusivity K_{eff} and Osborn–Cox diffusivity K_{OC} are related, as integrating the Osborn–Cox diffusivity along tracer contours is equivalent to the effective diffusivity. More formally, the effective diffusivity is derived by transforming the advection–diffusion Eq. (1) from Eulerian spatial coordinates to the Lagrangian area coordinate A . Transforming to area coordinates leads to the following diffusion-only equation

$$\frac{\partial q}{\partial t} = \frac{\partial}{\partial A} \left(K_{\text{eff}} \frac{\partial q}{\partial A} \right), \quad (2)$$

where the effective diffusivity K_{eff} is given by

$$K_{\text{eff}}(q, t) = \kappa \frac{\frac{d}{dA} \int_A |\nabla q(t)|^2 dA}{L_{\text{min}}^2 \left[\frac{\partial q(t)}{\partial A} \right]^2}, \quad (3)$$

where κ is the same prescribed model diffusivity from Eq. (1), and L_{min} is the minimum length of a tracer

contour. The effective diffusivity K_{eff} is a function of the tracer value q , and the area integral \int_A is computed over the region of $\tilde{q} < q$. The effective diffusivity has a corresponding across-contour flux F_{eff} , defined as [cf. Eq. (2.5b) in Nakamura (1996)]

$$F_{\text{eff}} = -\kappa \int_A (\nabla^2 q) dA, \quad (4)$$

and represents the total cross-contour transport.

Using Eq. (3), we calculate the time mean and annual means of K_{eff} for the passive tracer in both the upstream and downstream regions. Note that by calculating K_{eff} in subregions of the North Atlantic, we are assuming that there is negligible net tracer flux into (or out of) the region. As we initialize the passive tracer on the time-mean streamfunction, the mean flow approximately transports equal amounts of tracer in and out of the region. This would not be the case if the tracer was initialized on some other field, such as latitude—the adjustment of the tracer to the mean flow would cause large net fluxes in and out of the region.

Figures 2b and 2c shows the time-mean effective diffusivity for the upstream and downstream regions, respectively, as a function of tracer value q . The time-mean passive tracer field is shown in Fig. 2a to illustrate where each value of the tracer q occurs in the North Atlantic; in general, lower values of q correspond to more northerly latitudes. The essential difference between the upstream and downstream regions is that upstream exhibits a significant mixing barrier in the jet core (tracer values $q = 0.1 - 0.15$), with diffusivity values of $\approx 1 \times 10^3 \text{ m}^2 \text{ s}^{-1}$ (Fig. 2b). The downstream region however exhibits a single peak which reaches a value of $\approx 10 \times 10^3 \text{ m}^2 \text{ s}^{-1}$ (Fig. 2c). Therefore, the coherent Gulf Stream jet in the upstream region significantly suppresses mixing, but not the North Atlantic Current and Azores Current of the downstream region.

Despite the suppressed effective diffusivity in the upstream region, the magnitude of the cross-contour tracer flux is larger in the upstream region (Fig. 2d) relative to downstream (Fig. 2e)—note that negative values of the tracer flux indicate a net transport from positive to negative tracer values, which is primarily a poleward transport. Therefore, despite the mixing barrier, there is more across-jet exchange of tracer in the upstream region. This is due to the tracer gradients being significantly larger in the upstream region, as can be seen by the tightly packed contours in Fig. 2a. The large tracer gradients in the upstream region more than compensate for the decreased diffusivity when contributing to the total tracer flux.

The interannual variability of the diffusivity coefficient and flux is defined as the standard deviation of

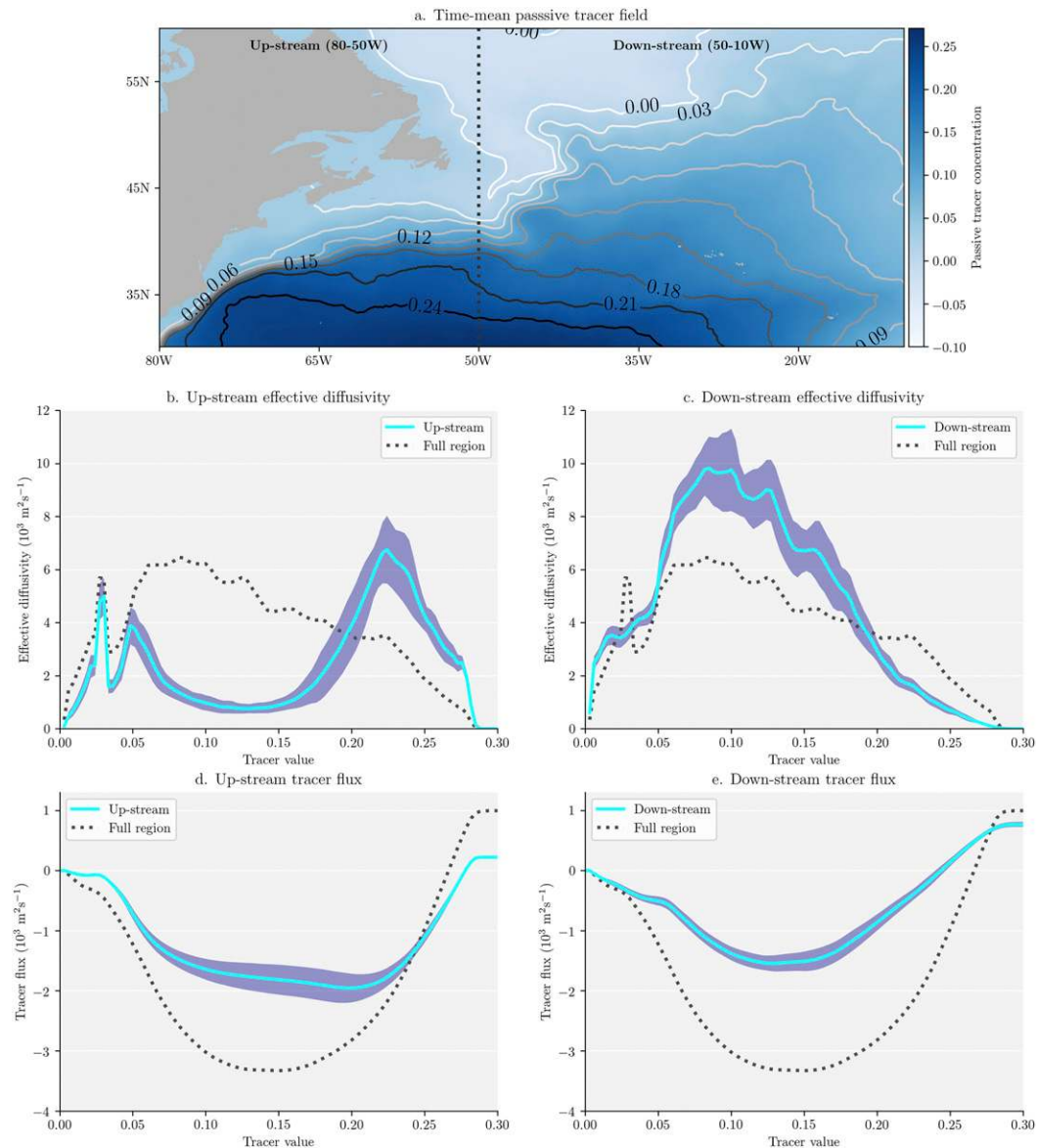


FIG. 2. The effective diffusivity, and the corresponding tracer flux, calculated for two different regions of the North Atlantic: upstream, defined as 80°–50°W, and downstream, defined as 50°–10°W. (a) The time-mean passive tracer field; the boundary between upstream and downstream is shown by the black dotted line. (b),(c) The effective diffusivity for the upstream and downstream regions, respectively; (d),(e) the corresponding tracer flux. The shading in (b)–(e) represents the interannual variability, defined as the standard deviation of the annual means. The black dotted lines in (b)–(e) illustrate the calculation over the full region.

the annual means and is illustrated by the shading in Figs. 2b–e. For both upstream and downstream, the interannual variability is 10%–20% of the time mean. The temporal variability of the effective diffusivity is more clearly illustrated in Figs. 3a and 3b, which shows the diffusivity as a function of time and tracer value for the upstream and downstream regions, respectively. Figure 3a shows that the mixing suppression effect in the upstream region is present in every year of the data, with

the single peak in the downstream region in Fig. 3b also present in every year. The along-stream variation in the diffusivities is therefore robust across all years of this experiment.

The individual time series of the jet core diffusivity ($q = 0.15$) are shown in Figs. 3c and 3d for the upstream and downstream regions, respectively. The upstream and downstream diffusivities at $q = 0.15$ vary independently of each other, with the upstream diffusivity

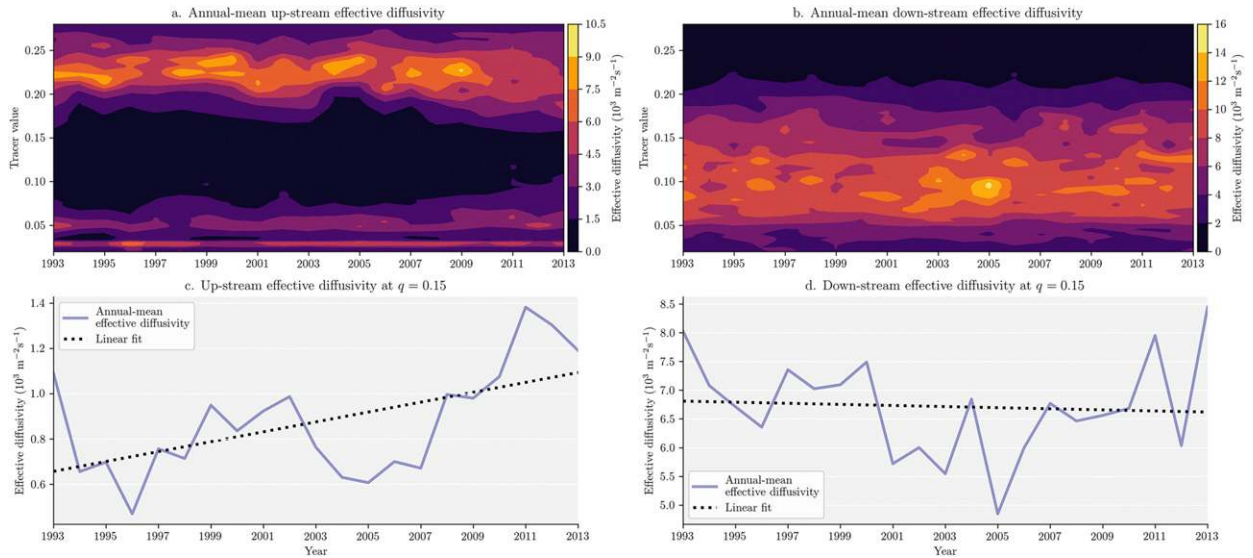


FIG. 3. (a),(b) The time evolution of the effective diffusivity as a function of tracer value (y axis) for the upstream and downstream regions, respectively. (c),(d) The individual time series at the tracer value $q = 0.15$, which is approximately collocated with the 25-cm SSH contour in the jet core. The black dotted lines in (c) and (d) are linear fits in time.

displaying long-term positive trend ($p < 0.05$) of $22 \text{ m}^2 \text{ s}^{-1} \text{ yr}^{-1}$.

c. Mixing length diffusivity expression

To determine the drivers of the observed temporal variability in Fig. 3, we diagnose a physically motivated expression for the lateral eddy diffusivity based on mixing length theory, which can be estimated from available satellite altimetry data. We employ the expression for the across-jet diffusivity derived by FN10, allowing us to link specific changes in the flow field to changes in the lateral mixing.

The FN10 diffusivity assumes a weakly nonlinear isotropic eddy field, takes into account the eddy phase speed c , the background zonal velocity U , and the root-mean-square (RMS) eddy velocity u_{rms} . The expression is given by

$$K_{\text{FN10}} = \frac{\Gamma L_e u_{\text{rms}}(t)}{1 + \frac{k^2}{\gamma^2} [U(t) - c]^2}, \quad (5)$$

where Γ is the mixing efficiency, L_e is the eddy length scale, γ is the reciprocal of the eddy decorrelation time scale, and $k = 2\pi/L_e$ is the eddy wavenumber. The denominator in this equation acts as a mixing suppression factor, which arises due to eddy propagation relative to the mean flow. The FN10 diffusivity [Eq. (5)] has been used to reproduce mixing rates in other areas of the ocean, where both jets and turbulent eddies are present (FN10; Klocker and Abernathy 2014).

The components that contribute most to the temporal variability of the lateral mixing based on FN10 will therefore reveal the important underlying dynamical processes driving effective diffusivity variability (Fig. 3). The various factors involved in the FN10 diffusivity expression are shown in Fig. 4, which are the following: the time-mean zonal velocity U ; the RMS eddy velocity u_{rms} , with eddy defined as deviation from the time mean; the eddy decorrelation time scale $\tau = 2\Gamma L_e / u_{\text{rms}}$ [Klocker and Abernathy 2014, their Eq. (8)]; and eddy phase speed c , where positive indicates westward propagation and is calculated from observational data using Radon transforms (C. Hughes 2018, personal communication). The resulting time-mean FN10 diffusivity K_{FN10} is shown in Fig. 4e. The time-mean FN10 diffusivity exhibits the mixing barrier effect upstream within the jet core at approximately $36^\circ\text{--}37^\circ\text{N}$, with increased values on the jet flanks. There is relatively little mixing suppression downstream, consistent with the effective diffusivity in Fig. 2.

To better compare the FN10 diffusivity with the effective diffusivity in Fig. 2, we average the FN10 diffusivity along SSH contours. This provides a quasi-Lagrangian perspective, similar to the use of the area coordinate in the effective diffusivity framework (Nakamura 1996). To do this, we calculate all the components of the FN10 diffusivity shown in Fig. 4 along SSH contours before calculating the final K_{FN10} expression. Therefore all quantities are calculated as a function of SSH, and not Eulerian spatial coordinates. Given the approximate nature of the formula, together with the spatial inhomogeneity of the input fields, we do not expect to obtain a perfect

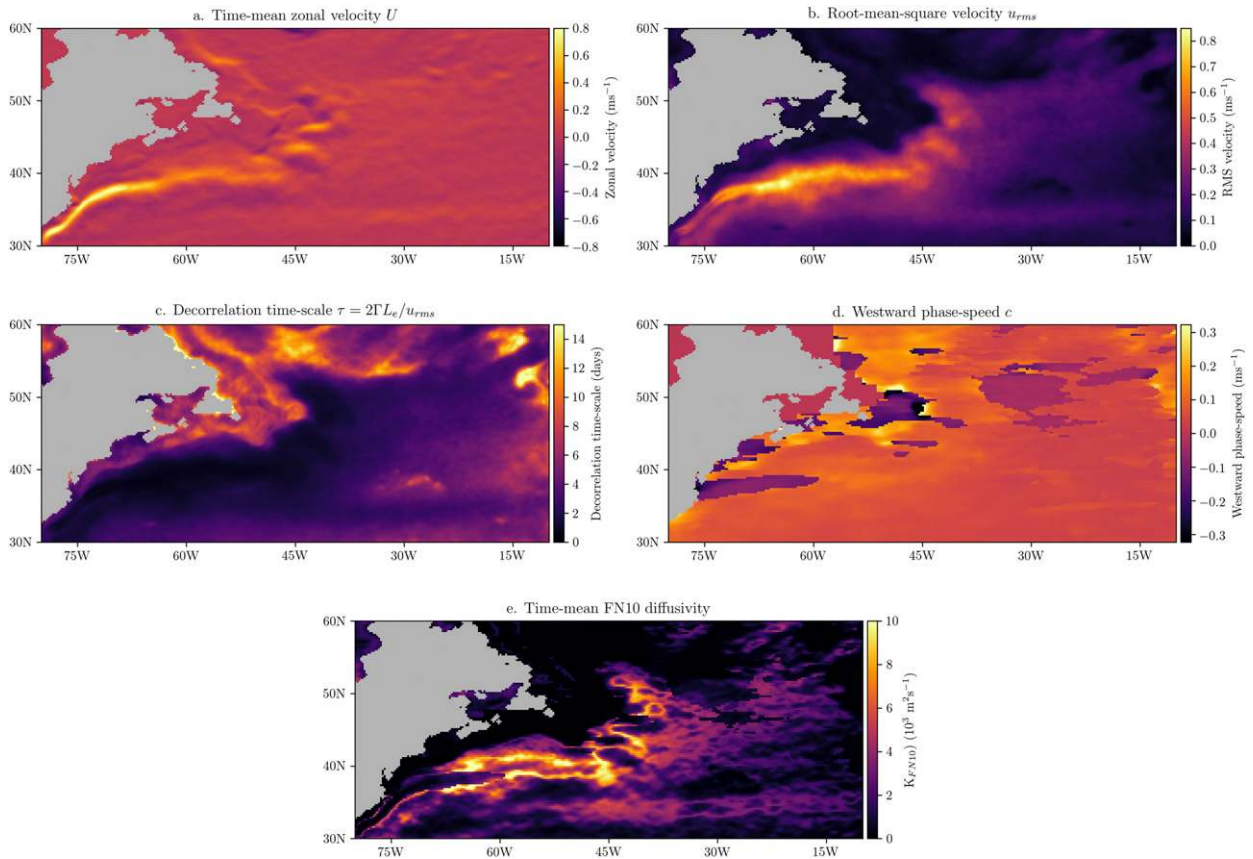


FIG. 4. The various components of the **FN10** diffusivity expression, calculated from satellite altimetry data. (a) The time-mean zonal velocity; (b) the RMS eddy velocity, where eddy is defined as the deviation from the time mean; (c) the decorrelation time scale in days, using the formula $\tau = 2\Gamma L_e/u_{rms}$; and (d) the eddy phase speed data, provided by C. Hughes (personal communication). (e) The final product: the time-mean diffusivity expression K_{FN10} .

quantitative match between K_{FN10} and K_{eff} in the Gulf Stream region. Rather, as mentioned above, our goal is to use the formula to gain physical understanding of what governs mixing and its variability.

The K_{FN10} diffusivity is shown as a function of SSH in Figs. 5b and 5c for the upstream and downstream regions, respectively, with the shading representing the interannual variability. In this coordinate, the mixing suppression of the upstream region is more evident in the K_{FN10} (although it is approximately double in the jet core compared to K_{eff}). The K_{FN10} diffusivity in the downstream region does not exhibit a mixing barrier, consistent with the along-stream variation observed with the effective diffusivity, but has a magnitude approximately 5 times smaller than K_{eff} .

Therefore the K_{FN10} diffusivity slightly overestimates the effective diffusivity in the upstream region and strongly underestimates the effective diffusivity in the downstream region. The overestimation of the mixing in the upstream region could be due to the nonzonal mean flow at the west side of the upstream region. Indeed, if this less zonal region is excluded, we do see slightly better agreement between

the effective and **FN10** diffusivities in the upstream region. The **FN10** diffusivity is therefore capturing the mixing barrier suppression in the upstream region.

The mismatch between effective diffusivity and **FN10** diffusivity downstream is more severe and could have been caused by nonlocal effects. The destabilized Gulf Stream jet in the upstream region may cause significant irreversible mixing of the passive tracer, which then propagates into the downstream region. Therefore effective diffusivity may interpret this change as an increased diffusivity in the downstream region, although the mixing actually occurred upstream.

However, we tested the sensitivity of the downstream effective diffusivity to changes in the dividing boundary separating upstream and downstream. We tested longitudes from 65° to 30° W (about the original longitude of 50° W). Regardless of the definition of the downstream region, the large peak in the effective diffusivity remains, implying that nonlocality does not contribute significantly to the observed peak in Fig. 2c. We also do not observe any relationship between the flux of tracer variance into

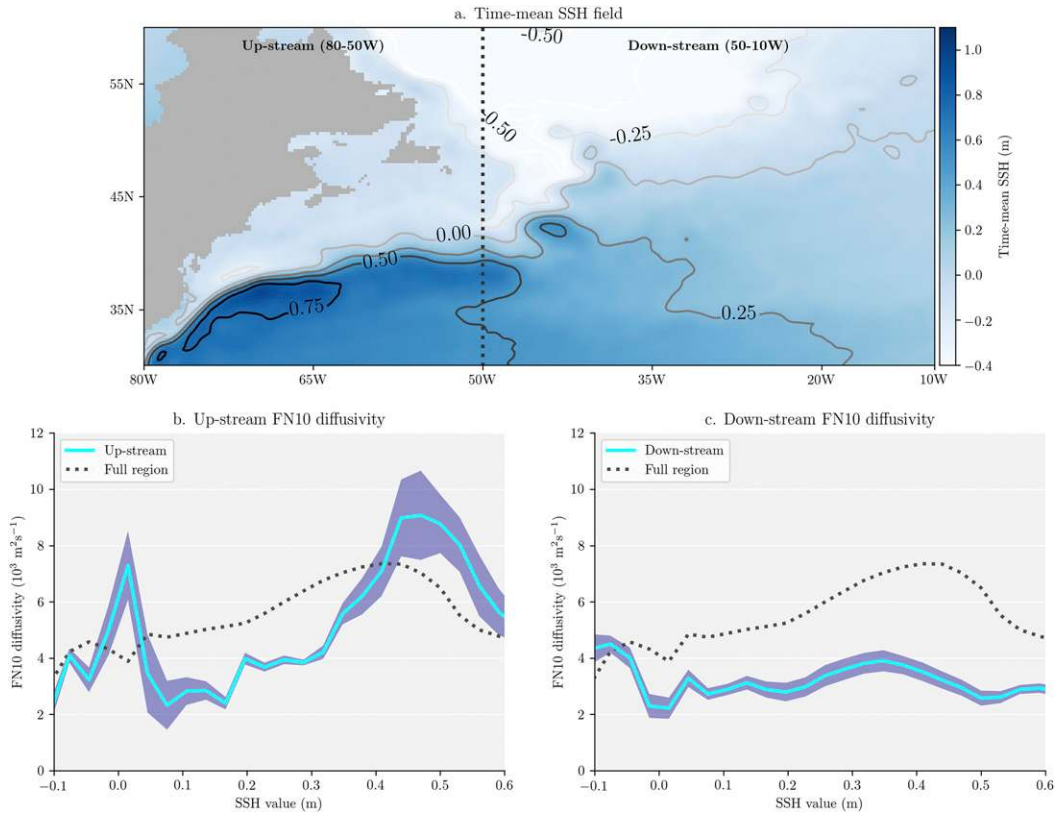


FIG. 5. (a) The time-mean SSH field from satellite altimetry data, illustrating where each SSH value is approximately located in the North Atlantic. (b),(c) The K_{FN10} diffusivity expression calculated along SSH contours. The shading represents the interannual variability, defined as the standard deviation of the annual means. The black dotted lines show the FN10 diffusivity calculated over the full region.

the downstream region and the diffusivity. These results suggest that the effective diffusivity is a robust indicator of mixing in these regions.

The mismatch may instead be due to the lack of time-scale separation between mean flow and eddies in the downstream region, which could cause large errors in the FN10 diffusivity. Consequently, the FN10 formula may not be capturing all the physical processes occurring in the downstream region.

To study the interannual variability in more detail, we can linearize the FN10 expression in Eq. (5) by assuming that only U and u_{rms} vary from year to year, while all other quantities remain constant. Perturbations to κ can then be written as the sum of contributions due to changes in the eddy velocity and the mean zonal velocity

$$\Delta K_{FN10} = \underbrace{\frac{\overline{K_{FN10}}}{\overline{u_{rms}}} \Delta u_{rms}}_{\text{Eddy perturbation}} - \underbrace{\overline{K_{FN10}} \frac{2k^2(\overline{U} - c)}{1 + \frac{k^2}{\gamma^2}(\overline{U} - c)^2}}_{\text{Mean perturbation}} \Delta U, \tag{6}$$

where we have decomposed the following variables into time means \bar{x} and annual deviations from the time mean Δx :

$$K_{FN10} = \overline{K_{FN10}} + \Delta K_{FN10}; \tag{7}$$

$$U = \overline{U} + \Delta U; \tag{8}$$

$$u_{rms} = \overline{u_{rms}} + \Delta u_{rms}. \tag{9}$$

The yearly linearized perturbations to the FN10 diffusivity for the upstream and downstream regions are shown in Figs. 6a and 6b, respectively. We focus on the FN10 diffusivity values along the 25-cm SSH contour (which represents the core of the jet in upstream region). The total perturbation to the FN10 diffusivity in the upstream region is dominated by perturbation from the mean flow ΔU . Indeed, the perturbation due to ΔU accounts for 98% of the total perturbation in the upstream region.

Downstream on the other hand shows more equal contributions to the total perturbation by the mean flow ΔU and eddy RMS velocity Δu_{rms} . As the currents are

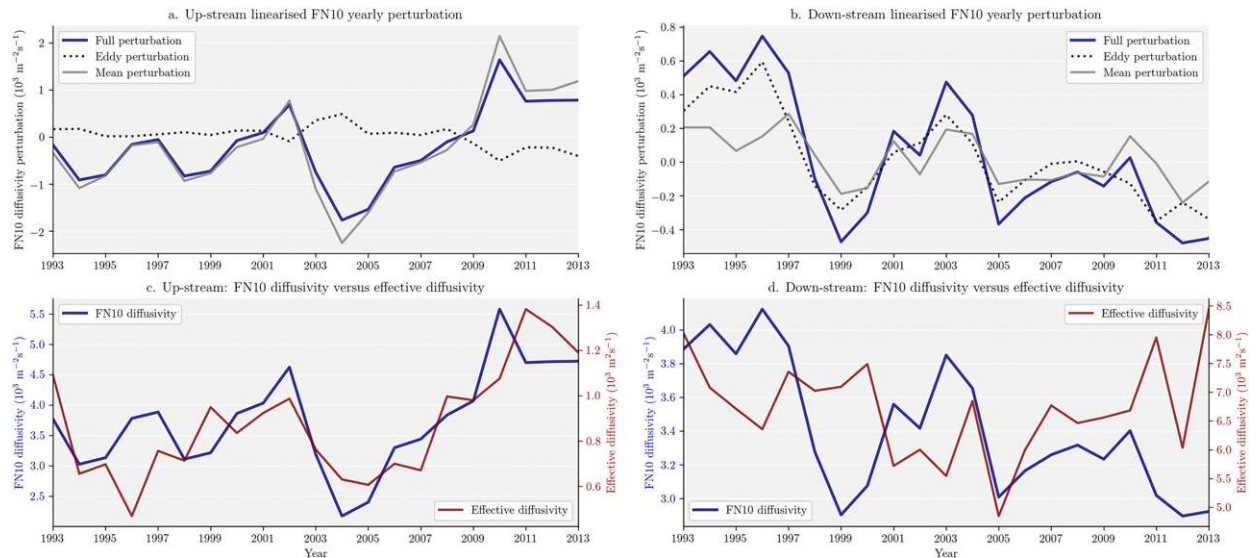


FIG. 6. (a),(b) Linear perturbations to the time-mean K_{FN10} diffusivity expression for both the upstream and downstream regions. (c),(d) Comparison of time series of the K_{FN10} diffusivity with the effective diffusivity in the jet core (at the 25-cm SSH contour for K_{FN10} and $q = 0.15$ for K_{eff}).

relatively weaker in the downstream region, the mean flow is more comparable in magnitude to the eddy velocity, both of which are also more comparable to the eddy phase speed. Therefore the temporal variability of the **FN10** diffusivity in the downstream region seems to be a more complex interplay between the mean flow, eddy velocity, and eddy phase speed.

Does the temporal variability of the **FN10** diffusivity match that of the effective diffusivity? We compare the individual time series of the effective diffusivity and **FN10** diffusivity in the upstream and downstream regions in Figs. 6c and 6d. We consider the 25-cm SSH contour for K_{FN10} , and the $q = 0.15$ tracer contour of K_{eff} ; both the 25-cm SSH contour and the $q = 0.15$ contour correspond to the jet core. The **FN10** diffusivity tracks the longer-term decadal variations in the effective diffusivity ($r = 0.75$, $p = 0.02$) for the upstream region, implying approximate agreement.

There is no relationship between the interannual variations in the **FN10** diffusivity and effective diffusivity in the downstream region ($r = -0.01$, $p = 0.5$). As discussed previously, nonlocal contributions to the effective diffusivity appear minimal. Therefore it may be the case that the **FN10** diffusivity expression does not accurately capture the correct physical processes in this region.

4. Upstream Gulf Stream jet dynamics

In Fig. 6, the linearized perturbations to the **FN10** diffusivity imply the mean flow is the dominant driver

of lateral mixing variability in the upstream region. The dynamics of the upstream region are dominated by a strong and coherent jet—do we see direct links between the dynamical properties of the jet and the diagnosed diffusivities?

We diagnose a quantity relevant to the mean flow for each year in the upstream region: the along-jet speed, defined as the average current speed along the 25 cm SSH contour, which provides a Lagrangian measure of “strength” in the jet core. Annual values of the along-jet speed are compared with annual values of the effective diffusivity and flux in Fig. 7.

Figure 7a shows there is a negative correlation ($r = -0.63$, $p < 0.01$) between the upstream effective diffusivity K_{eff} and along-jet speed. Figure 7b shows a positive correlation ($r = 0.51$, $p < 0.05$) between the upstream tracer flux and the along-jet speed (with a more negative tracer flux corresponding to an increase in the across-jet exchange of tracer). Overall these relationships show that, within the upstream region, a reduction in Gulf Stream mean flow is linked to increased across-jet tracer transport. We find similar results when using the area-average mean kinetic energy (MKE) as a diagnostic of mean flow.

No significant relationships were found between the regional-average eddy kinetic energy (EKE) and the effective diffusivity and tracer flux in the upstream region. The lack of relationship with EKE implies it is specifically the suppression of mixing by the mean flow that is the primary driver of across-jet transport variability in the upstream region. The result is consistent

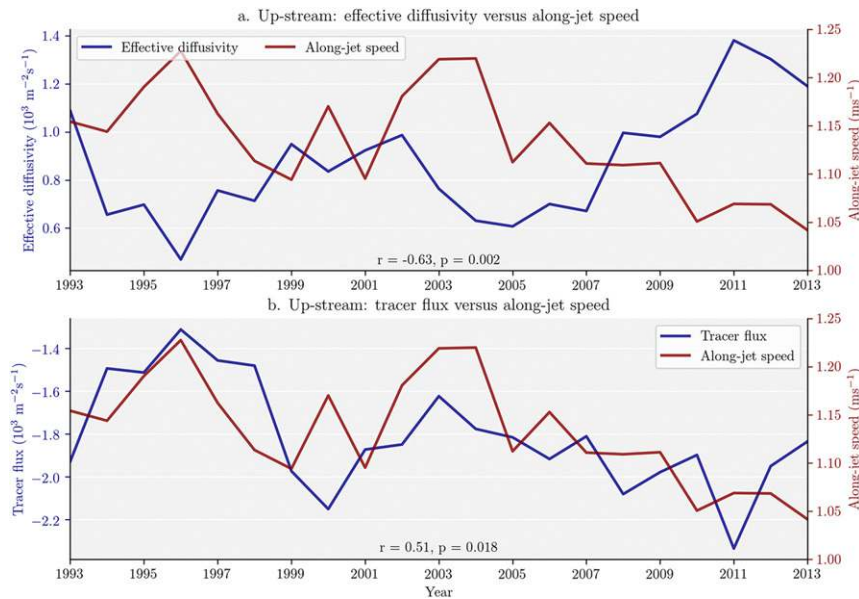


FIG. 7. Comparisons of the upstream effective diffusivity and tracer flux with a measure of mean flow: along-jet speed. Comparison of the (a) along-jet speed with the effective diffusivity and (b) along-jet speed with the tracer flux—both at the tracer value $q = 0.15$. Note that a more negative tracer flux indicates an increased across-jet exchange of the passive tracer.

with the analysis of linearized perturbations of the FN10 diffusivity in Fig. 6.

5. Discussion and summary

We investigated the interannual variability of the lateral mixing of a passive tracer in the North Atlantic, using an observation-driven passive tracer experiment in MITgcm. The passive tracer behaves similarly to observed SST (Fig. 1). Using the effective diffusivity of Nakamura (1996), we showed that lateral mixing at the surface exhibits significant along-stream variation in the North Atlantic (Fig. 2). In the upstream region (80° – 50° W), the Gulf Stream jet exhibits a suppressed diffusivity at the surface due to the strong mean flow (Fig. 2b), consistent with Bower et al. (1985). The North Atlantic Current and Azores current in the downstream region (50° – 10° W) however do not show any signs of reducing the effective diffusivity, which would occur if they were in fact suppressing mixing (Fig. 2c).

The interannual variability of the effective diffusivity is 10%–20% of the time mean (Fig. 2) for both the upstream and downstream regions. To determine the drivers of the temporal variability of the effective diffusivity, we used mixing length theory of FN10 to understand the physical controls on the across-jet diffusivity. The FN10 diffusivity successfully reproduces the mixing barrier in the upstream region (Fig. 5). In terms of the interannual variability, the FN10 diffusivity tracks the effective diffusivity

in the upstream region ($r = 0.75$, $p = 0.02$) (Fig. 6c), whereas the FN10 diffusivity in the downstream region does not match the effective diffusivity. ($r = -0.01$, $p = 0.5$) (Fig. 6d).

By assuming the mean flow and eddy velocity can vary from year to year, and linearly perturbing the FN10 diffusivity about the time mean, we determine what dynamical properties of the flow contribute to the interannual variability. We find that the perturbations due to the mean flow dominate the interannual variability in the upstream region (Fig. 6a), whereas downstream the mean flow and eddy velocity are more balanced in their contributions to the FN10 diffusivity (Fig. 6b).

The dominant role of the mean flow for the upstream FN10 diffusivity variability led us to look for direct links between Gulf Stream mean flow and the effective diffusivity. Using a measure of mean flow, the along-jet speed, we find an inverse relationship between jet strength and the amount of across-jet mixing: reduced mean flow leads to less suppression and more across-jet exchange of tracer on interannual time scales (Fig. 7).

The distinct mixing effects of the upstream and downstream regions show that a parameterization of eddy mixing must account for this along-stream variation. Yes, the FN10 diffusivity successfully accounts for the mean flow suppression in the upstream region, but it is still unclear what the primary drivers of mixing are in the downstream region. There is not a clear separation of mean flow and

eddies in the downstream region, which may contribute to the issue, as scale separation is an assumption of the FN10 diffusivity. An eddy parameterization must therefore be sensitive to the dynamical intricacies of each region.

Along-stream variation in the interactions of eddies has previously been studied in an idealized model (Waterman and Jayne 2010) and using observations of the Kuroshio Extension (Waterman et al. 2011): the upstream region is characterized by an unstable jet generating eddies, whereas downstream the jet radiates energy, known as the wave-maker regime. Liu et al. (2018) studied Lagrangian structure dynamics in the Gulf Stream using satellite altimetry data, in order to quantify transport and mixing. Lobes and eddy pinch-off were found to contribute to the across-jet transport, and this behavior was interpreted in terms of the unstable jet and wave-maker regimes of Waterman and Jayne (2010). These studies consider along-stream variation on the scale of 100 km, whereas here we have considered upstream and downstream variations on the order of 1000 km. Nonetheless our results and the aforementioned studies show that the along-stream variations in eddy interactions are an important component of the large-scale circulation, particularly in Western boundary currents.

The discrepancy between the effective diffusivity and the FN10 diffusivity in the downstream region—in both the time mean and interannual variability—requires further study. The linearized analysis of Fig. 6 indicates a more complex interaction between the mean flow, eddy velocity, and eddy phase speed, with regards to the temporal variability of mixing in the downstream region.

Our results only concern lateral mixing at the surface, whereas subsurface mixing is also an important component of tracer transport in the North Atlantic. The study of Bower et al. (1985) suggested that the mixing-barrier effect of the Gulf Stream may diminish with depth. However along-stream variation in subsurface mixing requires further study—how does the subsurface mixing vary between the upstream and downstream regions? How does the subsurface mixing vary on interannual time scales? These questions cannot be answered with satellite altimetry data alone. Indeed, Foukal and Lozier (2016) studied Lagrangian trajectories in the North Atlantic and suggested that it is the subsurface transport which is important for connecting the Gulf Stream with the subpolar gyre, and not transport at the surface—this was originally argued by Bower et al. (1985). For the Kuroshio Extension, whether the cross-jet transport increased with depth was dependent on along-stream position (Chen et al. 2014), and in the Southern Ocean, the local maximum of cross-jet mixing occurred between 1000 and 1500 m (Griesel et al. 2014).

The mean flow is the primary driver of mixing in the upstream region, but what causes the variability in the mean flow to begin with? We know that temporal variability in the surface transport of the Gulf Stream and Kuroshio Extension are inversely related to a quantity called “path stability” (Kelly et al. 2010, their Fig. 14). Path stability is defined as the standard deviation of jet path latitude over some time period. The path stability is therefore related to the amplitude of jet meandering and the instability mechanisms that generate the meandering. Recent work by Chen et al. (2017) showed that the transitioning from a stable to unstable state (i.e., increased jet latitude variance) of the Kuroshio Extension led to increased across-jet mixing.

We examined links between path stability and lateral mixing in the upstream region. We defined the path stability of the Gulf Stream using the standard deviation of the latitude of the 25-cm SSH contour, similar to Andres (2016). We found positive correlations between measures of path stability and the effective diffusivity ($r \approx 0.5$), but none were statistically significant ($p > 0.1$). We do however observe the inverse relationship between path stability and along-jet speed between 70° and 65°W on interannual time scales ($r = -0.73$, $p = 0.01$). There may indeed be a dynamical mechanism linking path stability and across-jet mixing in the Gulf Stream, but more data—from observations or eddy-resolving models—is needed to robustly determine the relationship.

Overall we have shown that the regional variations in the dynamics of eddies has a significant impact on the transport and mixing of tracers at the ocean’s surface. In some regions, mixing can indeed be parameterized as a simple function of mean flow strength. However, in other regions the picture is more complex, and parameterizations based solely on mean flow and EKE may not capture the mixing effects of mesoscale eddies. This regional variability must be investigated further if we are to understand how distributions of climatic tracers will change in the future, and how to parameterize them accurately within climate models.

Acknowledgments. This work was funded by the Natural Environment Research Council (NERC; Award NE/L002612/1). The altimeter products were produced by Ssalto/Duacs and distributed by AVISO, with support from Cnes (www.aviso.altimetry.fr/duacs). The bathymetry product was produced by National Geophysical Data Center, NESDIS, NOAA, U.S. Department of Commerce (doi:10.1594/PANGAEA.769615). R.P.A. acknowledges support from NSF Award OCE 1553593.

REFERENCES

- Abernathy, R. P., and J. Marshall, 2013: Global surface eddy diffusivities derived from satellite altimetry. *J. Geophys. Res. Oceans*, **118**, 901–916, <https://doi.org/10.1002/jgrc.20066>.
- Adcroft, A., and Coauthors, 2008: MITgcm user manual. MIT Department of Earth, Atmospheric and Planetary Sciences, http://mitgcm.org/public/r2_manual/latest/online_documents/manual.html.
- Andres, M., 2016: On the recent destabilization of the Gulf Stream path downstream of Cape Hatteras. *Geophys. Res. Lett.*, **43**, 9836–9842, <https://doi.org/10.1002/2016GL069966>.
- Bower, A. S., 1991: A simple kinematic mechanism for mixing fluid parcels across a meandering jet. *J. Phys. Oceanogr.*, **21**, 173–180, [https://doi.org/10.1175/1520-0485\(1991\)021<0173:ASKMFM>2.0.CO;2](https://doi.org/10.1175/1520-0485(1991)021<0173:ASKMFM>2.0.CO;2).
- , and T. Rossby, 1989: Evidence of cross-frontal exchange processes in the Gulf Stream based on isopycnal RAFOS float data. *J. Phys. Oceanogr.*, **19**, 1177–1190, [https://doi.org/10.1175/1520-0485\(1989\)019<1177:EOCFEP>2.0.CO;2](https://doi.org/10.1175/1520-0485(1989)019<1177:EOCFEP>2.0.CO;2).
- , H. T. Rossby, and J. L. Lillibridge, 1985: The Gulf Stream—Barrier or blender? *J. Phys. Oceanogr.*, **15**, 24–32, [https://doi.org/10.1175/1520-0485\(1985\)015<0024:TGSOB>2.0.CO;2](https://doi.org/10.1175/1520-0485(1985)015<0024:TGSOB>2.0.CO;2).
- Busecke, J. J., and R. P. Abernathy, 2019: Ocean mesoscale mixing linked to climate variability. *Sci. Adv.*, **5**, eaav5014, <https://doi.org/10.1126/sciadv.aav5014>.
- , —, and A. L. Gordon, 2017: Lateral eddy mixing in the subtropical salinity maxima of the global ocean. *J. Phys. Oceanogr.*, **47**, 737–754, <https://doi.org/10.1175/JPO-D-16-0215.1>.
- Chapman, C., and J.-B. Sallée, 2017: Isopycnal mixing suppression by the Antarctic circumpolar current and the southern ocean meridional overturning circulation. *J. Phys. Oceanogr.*, **47**, 2023–2045, <https://doi.org/10.1175/JPO-D-16-0263.1>.
- Chen, R., J. L. McClean, S. T. Gille, and A. Griesel, 2014: Isopycnal eddy diffusivities and critical layers in the Kuroshio extension from an eddying ocean model. *J. Phys. Oceanogr.*, **44**, 2191–2211, <https://doi.org/10.1175/JPO-D-13-0258.1>.
- , S. T. Gille, and J. L. McClean, 2017: Isopycnal eddy mixing across the Kuroshio Extension: Stable versus unstable states in an eddying model. *J. Geophys. Res. Oceans*, **122**, 4329–4345, <https://doi.org/10.1002/2016JC012164>.
- David, T. W., D. P. Marshall, and L. Zanna, 2017: The statistical nature of turbulent barotropic ocean jets. *Ocean Modell.*, **113**, 34–49, <https://doi.org/10.1016/j.ocemod.2017.03.008>.
- Ferrari, R., and C. Wunsch, 2009: Ocean circulation kinetic energy: Reservoirs, sources, and sinks. *Annu. Rev. Fluid Mech.*, **41**, 253–282, <https://doi.org/10.1146/annurev.fluid.40.111406.102139>.
- , and M. Nikurashin, 2010: Suppression of eddy diffusivity across jets in the southern ocean. *J. Phys. Oceanogr.*, **40**, 1501–1519, <https://doi.org/10.1175/2010JPO4278.1>.
- Foukal, N. P., and M. S. Lozier, 2016: No inter-gyre pathway for sea-surface temperature anomalies in the North Atlantic. *Nat. Commun.*, **7**, 11 333, <https://doi.org/10.1038/ncomms11333>.
- Gnanadesikan, A., M.-A. Pradal, and R. Abernathy, 2015: Isopycnal mixing by mesoscale eddies significantly impacts oceanic anthropogenic carbon uptake. *Geophys. Res. Lett.*, **42**, 4249–4255, <https://doi.org/10.1002/2015GL064100>.
- Griesel, A., J. McClean, S. Gille, J. Sprintall, and C. Eden, 2014: Eulerian and Lagrangian isopycnal eddy diffusivities in the southern ocean of an eddying model. *J. Phys. Oceanogr.*, **44**, 644–661, <https://doi.org/10.1175/JPO-D-13-039.1>.
- Guinehut, S., A. Dhompis, G. Larnicol, and P.-Y. Le Traon, 2012: High resolution 3-D temperature and salinity fields derived from in situ and satellite observations. *Ocean Sci.*, **8**, 845–857, <https://doi.org/10.5194/os-8-845-2012>.
- Hughes, C. W., A. F. Thompson, and C. Wilson, 2010: Identification of jets and mixing barriers from sea level and vorticity measurements using simple statistics. *Ocean Modell.*, **32**, 44–57, <https://doi.org/10.1016/j.ocemod.2009.10.004>.
- Kelly, K. A., R. J. Small, R. Samelson, B. Qiu, T. M. Joyce, Y.-O. Kwon, and M. F. Cronin, 2010: Western boundary currents and frontal air–sea interaction: Gulf Stream and Kuroshio Extension. *J. Climate*, **23**, 5644–5667, <https://doi.org/10.1175/2010JCLI3346.1>.
- Klocker, A., and R. Abernathy, 2014: Global patterns of mesoscale eddy properties and diffusivities. *J. Phys. Oceanogr.*, **44**, 1030–1046, <https://doi.org/10.1175/JPO-D-13-0159.1>.
- , R. Ferrari, and J. H. LaCasce, 2012: Estimating suppression of eddy mixing by mean flows. *J. Phys. Oceanogr.*, **42**, 1566–1576, <https://doi.org/10.1175/JPO-D-11-0205.1>.
- Le Traon, P., F. Nadal, and N. Ducet, 1998: An improved mapping method of multisatellite altimeter data. *J. Atmos. Oceanic Technol.*, **15**, 522–534, [https://doi.org/10.1175/1520-0426\(1998\)015<0522:AIMMOM>2.0.CO;2](https://doi.org/10.1175/1520-0426(1998)015<0522:AIMMOM>2.0.CO;2).
- Liu, Y., C. Wilson, M. A. Green, and C. W. Hughes, 2018: Gulf Stream transport and mixing processes via coherent structure dynamics. *J. Geophys. Res. Oceans*, **123**, 3014–3037, <https://doi.org/10.1002/2017JC013390>.
- Marshall, J., A. Adcroft, C. Hill, L. Perelman, and C. Heisey, 1997: A finite-volume, incompressible Navier Stokes model for studies of the ocean on parallel computers. *J. Geophys. Res.*, **102**, 5753–5766, <https://doi.org/10.1029/96JC02775>.
- , E. Shuckburgh, H. Jones, and C. Hill, 2006: Estimates and implications of surface eddy diffusivity in the Southern Ocean derived from tracer transport. *J. Phys. Oceanogr.*, **36**, 1806–1821, <https://doi.org/10.1175/JPO2949.1>.
- Nakamura, N., 1996: Two-dimensional mixing, edge formation, and permeability diagnosed in an area coordinate. *J. Atmos. Sci.*, **53**, 1524–1537, [https://doi.org/10.1175/1520-0469\(1996\)053<1524:TDMEFA>2.0.CO;2](https://doi.org/10.1175/1520-0469(1996)053<1524:TDMEFA>2.0.CO;2).
- Osborn, T. R., and C. S. Cox, 1972: Oceanic fine structure. *Geophys. Astrophys. Fluid Dyn.*, **3**, 321–345, <https://doi.org/10.1080/0309197208236085>.
- Rossby, T., 1996: The North Atlantic current and surrounding waters: At the crossroads. *Rev. Geophys.*, **34**, 463–481, <https://doi.org/10.1029/96RG02214>.
- Samelson, R., 1992: Fluid exchange across a meandering jet. *J. Phys. Oceanogr.*, **22**, 431–444, [https://doi.org/10.1175/1520-0485\(1992\)022<0431:FEAAMJ>2.0.CO;2](https://doi.org/10.1175/1520-0485(1992)022<0431:FEAAMJ>2.0.CO;2).
- Schmittner, A., and A. J. Weaver, 2001: Dependence of multiple climate states on ocean mixing parameters. *Geophys. Res. Lett.*, **28**, 1027–1030, <https://doi.org/10.1029/2000GL012410>.
- Shuckburgh, E., H. Jones, J. Marshall, and C. Hill, 2009: Understanding the regional variability of eddy diffusivity in the Pacific sector of the Southern Ocean. *J. Phys. Oceanogr.*, **39**, 2011–2023, <https://doi.org/10.1175/2009JPO4115.1>.
- Waterman, S., and S. R. Jayne, 2010: Eddy-mean flow interactions in the along-stream development of a western boundary current jet: An idealized model study. *J. Phys. Oceanogr.*, **41**, 682–707, <https://doi.org/10.1175/2010JPO4477.1>.
- , and B. J. Hoskins, 2013: Eddy shape, orientation, propagation, and mean flow feedback in western boundary current

- jets. *J. Phys. Oceanogr.*, **43**, 1666–1690, <https://doi.org/10.1175/JPO-D-12-0152.1>.
- , N. G. Hogg, and S. R. Jayne, 2011: Eddy–mean flow interaction in the Kuroshio Extension region. *J. Phys. Oceanogr.*, **41**, 1182–1208, <https://doi.org/10.1175/2010JPO4564.1>.
- Wortham, C., and C. Wunsch, 2014: A multidimensional spectral description of ocean variability. *J. Phys. Oceanogr.*, **44**, 944–966, <https://doi.org/10.1175/JPO-D-13-0113.1>.
- Yang, H., 1996: The subtropical/subpolar gyre exchange in the presence of annually migrating wind and a meandering jet: Water mass exchange. *J. Phys. Oceanogr.*, **26**, 115–130, [https://doi.org/10.1175/1520-0485\(1996\)026<0115:TSGEIT>2.0.CO;2](https://doi.org/10.1175/1520-0485(1996)026<0115:TSGEIT>2.0.CO;2).
- , and Z. Liu, 1994: Chaotic transport in a double gyre ocean. *Geophys. Res. Lett.*, **21**, 545–548, <https://doi.org/10.1029/94GL00306>.